Confining Effect due to Geosynthetics Wrapping Compacted Soil Specimen
geosynthetics로 보강된 다짐토 공시체의 구속효과

김은라[1] Kim, Eun-Ra, Atsushi Iizuka[2], 김유성[3] Kim, you-seong, 박홍[4] Park Hong

[1] 전북대학교 연구원, researcher, Chonbuk National University
[2] Associate Professor, Department of Architecture and Civil Engineering, Kobe University
[3] 전북대학교 토목공학과 부교수Associate Professor, Department of Civil Engineering, Chonbuk University
[4] LG건설 기술본부, LG construction Co.

개요(SYNOPSIS) : 본 연구에서는 geosynthetics로 보강된 다짐토의 보강 메카니즘을 파악하기 위한 목적으로 실내시험 및 수치계산 수행하였다. 본 연구에서 고려하는 보강 메카니즘은 전단에 의한 다짐토의 체적 팽창(부의 다일렌탄시)을 geosynthetics에 의해 구속 억제하는 과정에서 생성되는 효과로 생각한다. 먼저, 실내실험을 위한 구체적인 방법으로서, geosynthetics의 보강효과를 정량적으로 파악하기 위하여 사질토를 다짐하여 공시체를 만들어 그 주위에 geosynthetics를 설치하여 전체적으로 압축전단시험을 실시하였다. 또한, 다짐토의 다짐도를 달리 하고 한 가지 종류만의 geosynthetics를 이용하여, 다짐토와 geosynthetics의 상호작용에 따른 압축력 변화, geosynthetics의 인장력 변화 및 공시체의 파괴진행상황 등을 살펴보았다. 수치계산에서는 다짐토의 다일렌탄시 특성에 대하여 표현 가능한 탄소성 구성모델을 이용하였다. 또한, 탄소성 구성 모델에서 항복 이전의 탄성영역의 거동을 묘사하기 위하여 Hashiguchi(1989)가 제안한 subloading surface의 개념을 도입하였고, 유한요소(FEM)해석을 통해 얻어진 결과들을 실내시험의 결과와 비교 분석하였으며, 그 결과 양자 양호한 결과를 얻었다.
Keywords: Compacted soils, Geosynthetic-reinforcement, Elasto-plastic modeling

1. INTRODUCTION

This paper presents the modeling of geosynthetic-reinforced compacted soils and discusses the reinforcement effect arising from by confining the dilatancy deformation of the soil by geosynthetics. A series of compressive shear tests for compacted sandy soil specimens wrapped by geosynthetics is carried out by quantitatively examining the geosynthetic-reinforcement effect, and it occurred from the confinement of the dilative deformation of compacted soils during shearing. In the test, the initial degree of compaction is changed for each series of sandy soil specimens so that each series has different degree of dilatancy characteristics. Herein, the axial forces working to the geosynthetics so as to prevent dilative deformation of compacted soils during shearing are measured. The behavior of the geosynthetic-reinforced soil structure is governed by the mechanical interaction between compacted soil and geosynthetic material and the treatment as an initial boundary value problem is required. Namely, we cannot discuss the geosynthetic-reinforcement effect only from the (limit) equilibrium of forces as seeing in the conventional design method. Therefore, it is necessary to treat the geosynthetic-reinforcement mechanism under the theoretical framework of the constitutive equations both compacted soils and geosynthetics, which was prepared as a mediator between the equilibrium of forces and strain compatibility. In this

paper, the authors introduce the elasto-plastic constitutive model to which the subloading surface concept proposed by Hashiguchi (1989) is installed to describe the mechanical properties of compacted soils. The geosynthetic material can be simply modeled to have elastic characteristics, based on the extension test result.

2. COMPRESSIVE SHEAR TEST

The soil used in experiment is the Pleistocene sand named Omma sand, sampled from Taiyogaoka, Kanazawa, Japan. The specific gravity of soil particle is 2.74, the grain size distribution is the gravel fraction (2 to 75 mm) of 2%, the sand fraction (75mm to 2 mm) of 80%, the silt fraction (5mm to 75 mm) of 11% and the clay fraction (less than 5 mm) of 7 %, respectively. The uniformity coefficient is 21.8 and the maximum grain size is 9.5 mm.

The Omma sand with the prescribed water was uniformly compacted by rammer of 3.5 kg up to a designated degree of compaction, and it was wrapped by geosynthetics as shown in Fig.3. The soil is spread in the thickness of 40 to 80 mm for each compaction. The compacted soil specimen (30 cm in diameter and 40cm in height) was laid on the uniaxial loading apparatus as shown in Fig.4 and was subjected to compressive shear(Iizuka et al., 2002). Table 1 summarizes the prepared compacted soil specimens for the test. The number of compaction and the spread thickness were varied with the specimen as shown in Table 1. Some specimens with lower degree of compaction (tests 6 to 8 in Table 1) were also prepared to investigate the influence on the geosynthetic-reinforcement effect due to the difference of the dilatancy characteristics of compacted soil. Herein, in order to measure the extension forces working on geosynthetics, strain gauges are tightly pasted on the geosynthetics as shown in Fig.1. In the experiment, the vertical displacement of the specimen and the extension stress working on the geosynthetics were measured by using the applied vertical load as shown in Fig.2. The compressive shear was carried out at the sufficiently slow rate in order to satisfy the condition that the volume of specimen is changeable (drained condition).

Table 1 Prepared specimens

test No	degree of compaction(the number of compaction)×(layers)	water content w(%)	dry density $\rho_d(g/cm^3)$
2	50×10	18.1	1.53
3	50×10	17.6	1.56
4	50×10	17.3	1.60
5	50×10	17.1	1.54
6	30×6	16.6	1.43
7	30×6	17.0	1.43
8	25×5	16.8	1.45
9	50×10	16.5	1.55

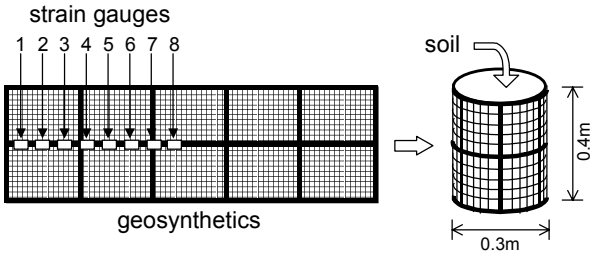

Fig. 1 Preparation of test specimens

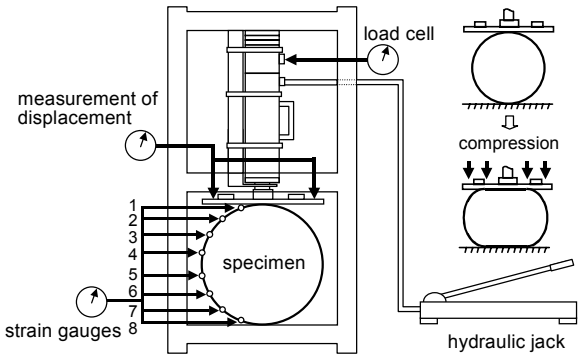

Fig. 2 Compressive shear apparatus

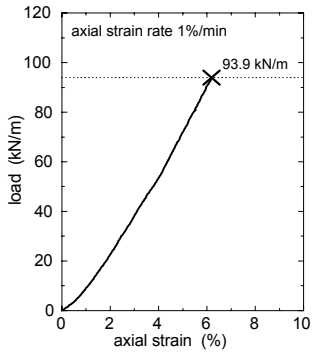

Fig. 3 Stress-strain relation of geosynthetics

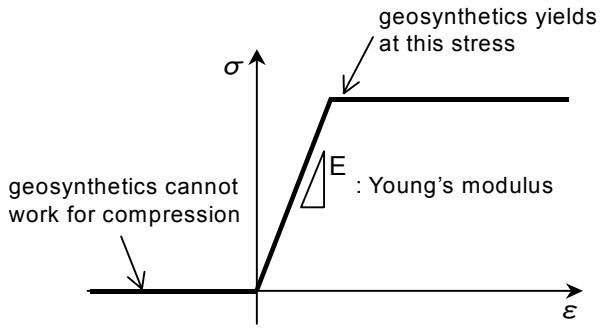

Fig.4 Geosynthetics model (bar element)

In the geosynthetic materials used in the experiment, the uniaxial extension test was carried out to measure the stiffness and the ultimate strength of the geosynthetics. Fig.3 shows the stress-strain relation of geosynthetic material obtained from the uniaxial extension test. The extension strength is 93.9kN/m, the cross sectional area is $3.2\times10^{-4}m^2$ and Young's modulus is $4.86\times10^{6}kPa$, respectively. The geosynthetic have to be modeled as a linearly elastic material as shown in Fig.4.

3. ELASTO-PLASTIC MODELING OF COMPACTED SOIL

They have some difficulties in expressing the mechanical behavior inside the normal yielding surface. Moreover, some additional parameters have to be determined. This is a big obstacle to the use of practical engineering at the present stage.

Therefore, we introduce the conventional elasto-plastic constitutive model(Sekiguchi and Ohta ,1977) and the subloading surface concept(Hashiguchi, 1989) to understand the mechanical behavior inside the normal yielding surface. The constitutive model by Sekiguchi and Ohta (1977) can be regarded as an extension of the original Cam clay model but is distinguished from the Cam-clay model on description ability of the mechanical behavior, which arose from initial anisotropyand stress reorientation. The determination procedure of input parameters needed in the constitutive model has been well established (Iizuka and Ohta,1987) through a lot of practical case studies using a finite element code, DACSAR, which is employed in the Sekiguchi and Ohta's model (Iizuka and Ohta, 1987 and Mestat, 2001).

3.1 Sekiguchi and Ohta's model with subloading surface

The normal yielding function of the Sekiguchi and Ohta's model is expressed as,

$$f=\frac{\lambda-\kappa}{1+e_0}\ln\frac{p'}{p'_0}+D\eta^*-\varepsilon_v^p=0 \tag{1}$$

where D is the coefficient of dilatancy(Shibata, 1968), ε_v^p is the volumetric strain, $\lambda(=0.434C_c)$ and $\kappa(=0.434C_s)$ are compression and swelling indices, respectively. The parameters of λ, κ and D have a theoretical relation with the critical state parameter, M, as $M=\frac{\lambda-\kappa}{D(1+e_0)}$ (Ohta, 1971). η^* is the generalized deviatoric stress parameter defined as,

$$\eta^*=\sqrt{\frac{3}{2}}\left\|\frac{\mathbf{s}}{p'}-\frac{\mathbf{s}_0}{p'_0}\right\| \tag{2}$$

where $\mathbf{s}$ is the deviatoric stress tensor, the subscript 0 denotes the value at the reference and $\|\cdot\|$ is the Euclid norm. After Hashiguchi (1989), the subloading surface f_s similar to the normal yielding surface can be defined using the similarity ratio R, as,

$$f_s=\frac{\lambda-\kappa}{1+e_0}\ln\frac{p'}{p'_0}+D\eta^*-\left(\varepsilon_v^p+\frac{\lambda-\kappa}{1+e_0}\ln R\right)=0 \tag{3}$$

where the similarity ratio R determines the scale of subloading yielding surface against the normal yielding surface and is defined as $p'/\overline{p}'$ using the current effective mean stress, p' on the subloading yielding surface and its conjugate effective mean stress, $\overline{p}'$ on the normal yielding surface. The evaluation law of the similarity ratio, R is assumed as,

$$\dot{R} = U_R \left\| \dot{\boldsymbol{\varepsilon}}^p \right\| = -\frac{m}{D}(\ln R)\left\| \dot{\boldsymbol{\varepsilon}}^p \right\| \quad \text{for } \dot{\boldsymbol{\varepsilon}}^p \neq \mathbf{0}. \quad (4)$$

After Hashiguchi (1989), the parameter m is the newly introduced material parameter controlling the accessibility rate of the subloading surface to the normal yielding surface. Herein, note that the scalar function, U_R is defined in the region of $0 < R \leq 1$ and satisfies $U_R = \infty$ at $R=0$ and $U_R = 0$ at $R=1$.

3.2 Calibration of modeling

In this section, the simulation of shear behavior obtained from SBT under the condition of constant volume is presented. The input parameters are determined from the compression test and the shear test results for disturbed sample. The stress ratio, $(\tau/\sigma'_v)_f$ at the critical state in case of the direct shearing such as the shear box test under the condition of constant volume, can be derived by simultaneously solving the critical state condition, and the undrained (constant volume) condition, $\dot{\epsilon}_v (= \dot{\epsilon}_v^e + \dot{\epsilon}_v^p) = 0$ of Sekiguchi and Ohta's model as (Ohta et al., 1993 and Morikawa et al., 1997),

$$\left(\frac{\tau}{\sigma'_v}\right)_f = \frac{1+2K_0}{3\sqrt{3}} M \quad (5)$$

With the help of empirical relation of $K_0 = 1 - sin\phi'$(Jaky, 1944), the critical state parameter, M can be expressed by $(\tau/\sigma'_v)_f$ at $M = \frac{6sin\phi'}{3-sin\phi'}$. The experimental value of $(\tau/\sigma'_v)_f$ is given in shear characteristics, though little difference is found in the critical state lines with the water content.

Herein, the kink point of effective stress path is chosen as the critical state point and then the critical state parameter, M is determined to be 1.42. The compression index, $\lambda (= 0.434 C_c)$ can be directly determined to be 0.12 from compression characteristics of disturbed samples because it is known that the gradient of compression line from Ko consolidation in the $e - ln\sigma_v'$ relation and that from the isotropic consolidation in the $e - lnp'$ relation coincides with each other (e.g., Mitachi and Kitago, 1976). And the swelling index, κ is estimated as 0.023 from the empirical relation of $M = 1.75(1 - \kappa/\lambda)$ (Karube, 1975), since the swelling index required as an input parameter in the constitutive model is the gradient of the isotropic swelling line. But, here, it differs from that of Ko swelling line shown in compression characteristics of undisturbed samples. The equivalent preconsolidation vertical stresses are determined from Fig.5 with each of water contents. The lateral axis of effective normal stress is rewritten with a logarithm scale and Ko swelling data in compression characteristics of undisturbed samples are plotted in Fig.5, together with the virgin compression lines.

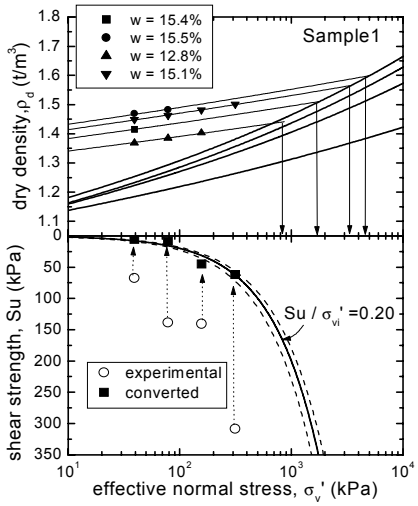

Fig. 5 Estimation of consolidation yield stress

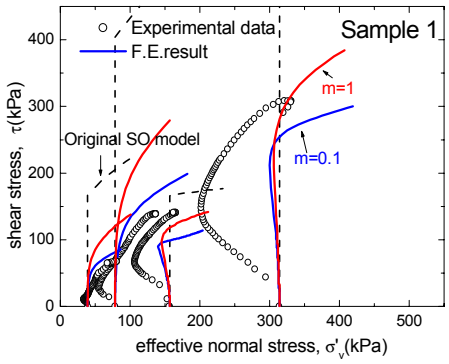

Fig.6 Computed stress paths of compacted soil

The value of equivalent preconsolidation vertical stress is given as each intersection of Ko swelling line and the virgin compression line with each water content value. The equivalent OCR is calculated as $\sigma'_{v0}/\sigma'_{vi}$ from the equivalent preconsolidation vertical stress and the current effective vertical stress. The coefficient of the current earth pressure at rest, K_i is estimated from the empirical relation of $K_i=(OCR)^n K_0$ and n=0.42 (Ladd et al., 1977). Then, the assumed Poisson ratio, ν is 0.33.

The theoretical effective stress paths computed from the Sekiguchi and Ohta's model with the subloading surface using the above-determined input parameters are compared in Fig.6 with the experimental results of shear characteristics of undisturbed samples, in which the parameter, m defined in Eq.(4) are assumed to be 1.0 and 0.1. And the theoretical paths computed from the original Sekiguchi and Ohta's model without introducing the subloading surface are also compared. It cannot be said that the computed prediction well explains the shear behavior of compacted soil. But at least, it can successfully express the dilatancy characteristics of compacted soil and the case of $m=1.0$ seems to give better prediction for the compacted Omma sand.

4. FINITE ELEMENT SIMULATIONS

4.1 Condition of analysis and preliminary elastic simulation

A series of finite element simulation of the compressive shear model tests was carried out. Figure 9 shows the finite element modeling of the test, where quadrilateral constant strain element with 4 nodes is employed. To simulate the compressive shear tests, the displacement is vertically installed to the specimen at the strain rate of 1.0 %/min as indicated in Fig.7.

First, as a preliminary simulation, the compacted soil is regard as a linearly elastic

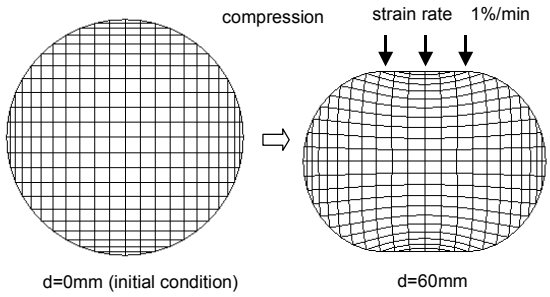

Fig.7 Finite element mesh employ

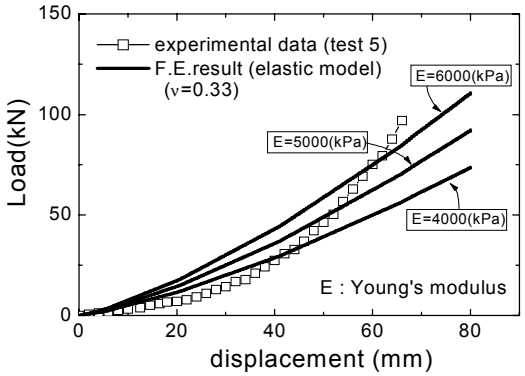

Fig.8 Computed load and displacement relation

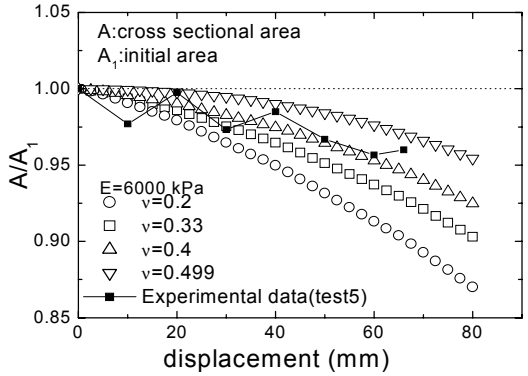

Fig.9 Computed cross sectional area (elastic)

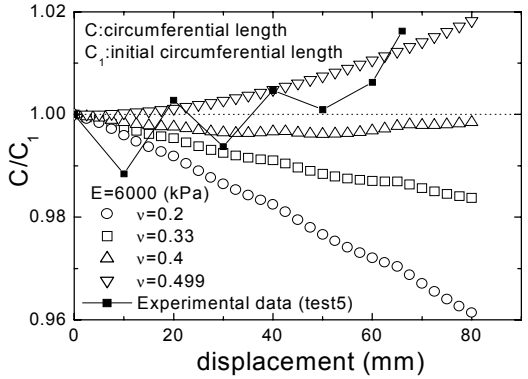

Fig.10 Computed circumference length (elastic)

material thathas no irreversible dilatancy characteristics associated with shearing. And also, based on the uniaxial extension test result of geosynthetics (Fig.3), the geosynthetics wrapping the soil specimen is modeled by linear elastic bar elements as shown in Fig.4. The properties are the young's modulus of $E=4.86\times10^{6}$ kPa, the cross sectional area of $A=3.2\times10^{-4}m^{2}$ and the compression strength of Nf=93.9 kN/m, respectively. In the computation, it is assumed that the bar elements (modeling the geosynthetics) do not resist against the axial compression as indicated in Fig.6.

Figure 8 compares the load and displacement relation obtained from the experiments with the computed ones. Here, three values of the young's modulus for the compacted soil are chosen as shown in the figure but the Poisson ratio is uniquely assumed to be 0.33 in all cases. The case of E=6000 kPa seems to well explain the load and displacement relation of well-compacted specimen, test 5 (see, Table 1). The change of cross sectional area and the change of circumference length of specimen are compared in Figs.9 and 10, respectively. The young's modulus of 6000 kPa is used in the computation because the case well explains the load and displacement relation, but the poisson ratio is varied from 0.2 to 0.499 at each of cases. As for the change of cross sectional area of the specimen in Fig.9, all the cases can be described the tendency showing the experiments(decrease of cross sectional area with loading). However, for the change of circumference length of the specimen as shown in Fig.10, only the case of ν'=0.499 can explain the experimental result of test 5.

The assumption of ν'=0.499 theoretically means the almost incompressibility condition and cannot be accepted as the poisson ratio of soil materials in the engineering practice. Fig.11 compares the computed distribution of extension forces working to the geosynthetics with the measured ones in test 5. From the figure, the elastic assumption without considering the dilatancy characteristics during the compressive shearing for the compacted soil cannot explain the geosynthetic-reinforcement effect observed in the model test.

4.2 Elasto-plastic finite element simulation

The material parameters needed in the elasto-plastic modeling of the compacted soil was already determined in the previous section. Now, it is necessary to estimate the equivalent preconsolidation vertical stresses in the compressive shear model tests. Figure 12 indicates the procedure to estimate the equivalent preconsolidation vertical stress considering the water content.

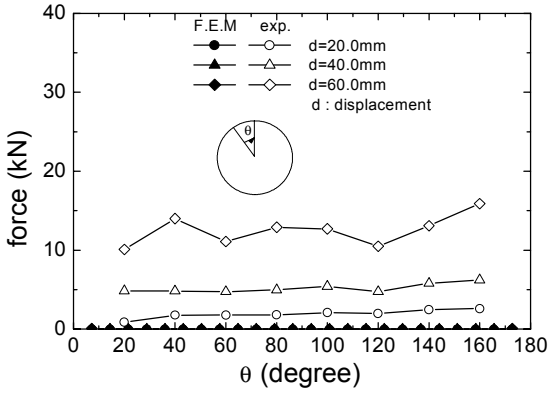

Fig.11 Extension forces along circumference of specimen(elastic)(E=6000 kPa and υ=0.33 for test5)

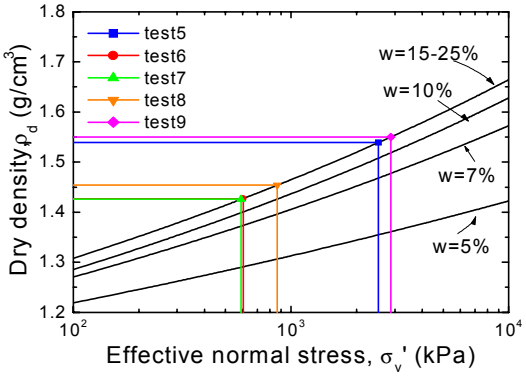

Fig.12 Estimate of equivalent preconsolidation stress

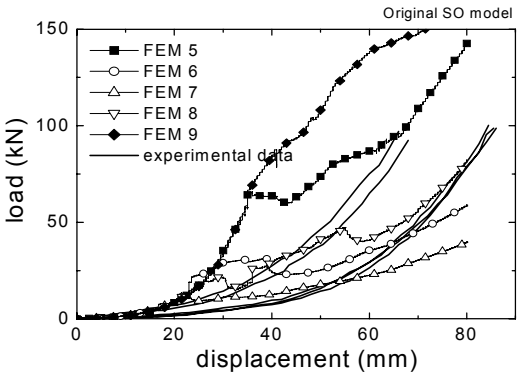

(a) Original Sekiguchi and Ohta's model

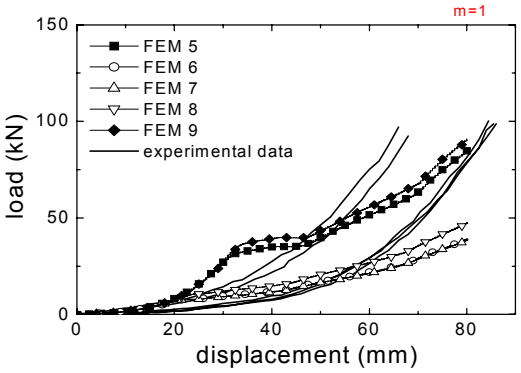

(b) Subloading model with m=1

Fig.13 Computed load and displacement relation

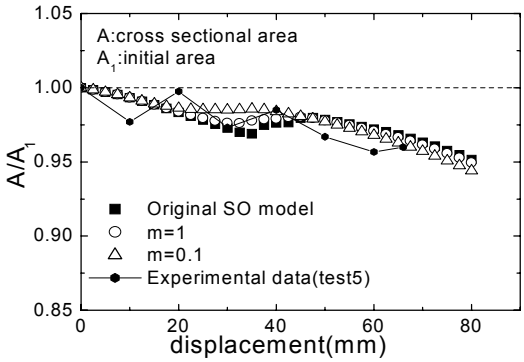

Fig.14 Computed cross sectional area

Since the evaluation of the initial effective vertical stresses in the specimen just before the compressive shear in the model test was very difficult, it was determined the equivalent preconsolidation vertical stress as the value corresponding to the initial dry density of each specimen as shown in Fig.5, which was not considered the slope of swelling line. Although the initial effective vertical stress, in reality, would be not uniform but is distributed in the specimen, the effective overburden pressure estimated at the center of specimen is employed in the computation as a representative value.

Figure 13 compares the computed load and displacement relation with the experimental results. In the figure, the black symbols, FEM 5 and FEM 9, denote the cases of well compacted specimen (high degree of compaction), corresponding to Test 5 and Test 9, respectively, while white symbols, FEM 6, FEM 7 and FEM 8, represent the cases of relatively poorly compacted specimen (relatively low degree of compaction), corresponding to Test 6, Test 7 and Test 8, respectively. Although the complete agreement between the computed and the measured results cannot be seen, it is found that the computed results, at least, explain the influence due to the difference of compaction degree. Moreover, it is found that introducing the subloading surface inside the normal yielding surface brings about smoother development of load and displacement curves, similar to the experimental results. Especially, the case of $m=1.0$, which controls the accessibility rate of the subloading surface to the normal yielding surface as defined in Eq.(4), seems to give better prediction.

Figs.14 and 15 compare the computed cross sectional area and circumference length of the specimen with the measured results (test 5). It can be seen that the computed predictions well explain the measured results.

Figure 16 indicates the computed development of axial forces working on the geosynthetics with the displacement at the locations of the strain gauges No.2 and compared with the measured results. And, Figure 17 show the computed distribution of axial forces along the circumference of the specimen, in which the case of high compaction degree (Test 5, FEM 5) is shown in Fig.13.

5. CONCLUSION

This paper presents the methodology and the tool to analyze the geosynthetic-reinforced soil structures and discusses the confining effect due to the geosynthetics wrapping the compacted soil specimen by conducting a series of the compressive shear model tests and the finite element simulations. Particularly the mechanical interaction between the compacted soils and the geosynthetic-reinforcement materials is emphasized as a benchmark that should be taken into consideration in analyzing the geosynthetic-reinforcement effect. Major items presented in this paper are summarized as follows.

1. The dilatancy characteristics of compacted soils depending on the degree of compaction are discussed. A trail to quantitatively express the degree of compaction by introducing the equivalent preconsolidation stress is presented.
2. The elasto-plastic constitutive modeling with the subloading surface is introduced to describe the mechanical behavior of compacted soils and its applicability to the compacted soils is examined.
3. A series of compressive shear tests for the compacted soil specimens wrapped by the geosynthetics is carried out and the geosynthetic-reinforcement effect is also examined.
4. A series of elasto-plastic finite element simulation of the compressive shear tests is performed and the applicability of the simulation technique to the analysis of the geosynthetic-reinforcement mechanism is examined by comparing the computed prediction with the measured results.

REFERENCES

1. Hashiguchi,K., 1989. Subloading surface model in unconventional plasticity, Int. J. of Solids and Structures, Vol.25, pp.917-945
2. Iizuka, A., Ohta, H., 1987. A deformation procedure of input parameters in elasto-viscoplastic finite element analysis, Soils and Foundations, Vol.27, No.3, pp.71-87
3. Iizuka, A., Hirata, M., Yokota, Y., Ohta, H., Kim, E.R., Kubo, T., 2002. Compressive shear tests of compacted soils wrapped by geosynthetics, Proc of 7th International Conference on Geosynthetics, IGS, Vol.3, pp.1133-1136

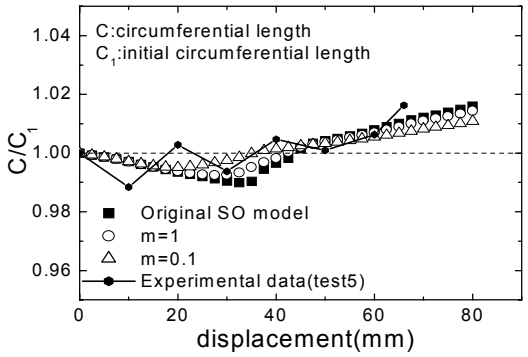

Fig.15 Computed circumference length

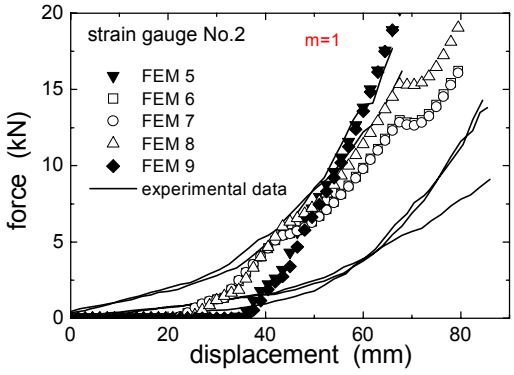

Fig.16 Extension forces (NO.2)

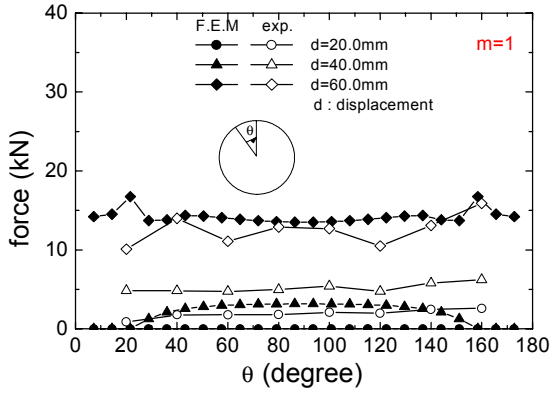

Fig.17 Extension forces along circumference of specimen(Test5)